Structural phase transition in the ordered fluorides $M^{II}ZrF_6$ (M^{II}=Co,Zn). I. Structural study

1990 J. Phys.: Condens. Matter 2 7373

(http://iopscience.iop.org/0953-8984/2/36/001)

J. Phys.: Condens. Matter 2 (1990) 7373–7386. Printed in the UK

Structural phase transition in the ordered fluorides $M^{II}ZrF_6$ (M^{II} = Co, Zn): I. Structural study

V Rodriguez†, M Couzi†, A Tressaud‡, J Grannec‡, J P Chaminade‡ and J L Soubeyroux§

† Laboratoire de Spectroscopie Moléculaire et Cristalline (URA124 CNRS), Université de Bordeaux I, 33405 Talence Cédex, France

‡ Laboratoire de Chimie du Solide du CNRS (CNRS), Université de Bordeaux I, 33405 Talence Cédex, France

§ Institut Laüe–Langevin, BP 156X, 38042 Grenoble Cédex, France

Received 6 February 1990, in final form 8 May 1990

Abstract. The mixed fluorides with formula $M^{II}ZrF_6$ (M^{II} = Co, Zn) exhibit an ordered ReO_3-type structure: this structure is made of a three-dimensional arrangement of corner-shared octahedra with an ordered distribution of M^{II} and Zr^{IV} cations in the octahedra sites. These materials undergo around room temperature a first-order ferroelastic structural phase transition from a cubic phase ($Fm\bar{3}m$) to a rhombohedral modification ($R\bar{3}$), as established by neutron and x-ray diffraction experiments. From a structural determination of $CoZrF_6$ at different temperatures through the phase transition, three order parameters have been measured, which enable one to describe completely the extent of lattice distortion in the rhombohedral phase: the spontaneous strain e_s, the coordinate of octahedra rotation around the threefold axis R and the octahedra internal deformation coordinate Q. Important thermal variations are observed for e_s and R, but the coordinate Q always remains very small, showing that the $Co(Zr)F_6$ octahedra are essentially rigid bodies. X-ray diffuse scattering experiments on $CoZrF_6$ at room temperature (cubic phase) are consistent with the existence of structural disorder due to rotations of the $Co(Zr)F_6$ octahedra around the cubic fourfold axes.

1. Introduction

The mixed fluorides with formula $M^{II}M'^{IV}F_6$ generally exhibit an ordered ReO_3-type structure with NaCl packing, which consists of $M^{II}(M'^{IV})F_6$ octahedra sharing corners in a three-dimensional array, and with M^{II} and M'^{IV} cations occupying alternately the octahedral holes (see for instance [1, 2] and the references cited therein) (figure 1). The parent phase ($NaSbF_6$ type) has cubic symmetry, with $Fm\bar{3}m$ space group and $Z = 4$ formula units in the crystallographic unit cell [3]. A structural phase transition from this cubic high-temperature form to a low-temperature form of the $LiSbF_6$ type [4], with $R\bar{3}$ space group and $Z = 1$, generally occurs in the 150–500 K temperature range [5]. From symmetry considerations, this phase transition is ferrodistortive–ferroelastic.

Another rhombohedral structure has been reported for a number of $M^{II}M'^{IV}F_6$ ($BaSiF_6$) and $M^{I}M'^{V}F_6$ ($KOsF_6$) ordered fluorides, consisting of a slightly distorted CsCl arrangement of M and isolated $M'F_6$ octahedra [1]. X-ray diffraction and vibrational studies of such mixed $MM'F_6$ have been interpreted in terms of $R\bar{3}m$ or $R\bar{3}$ space group with $Z = 1$; the choice between $R\bar{3}m$ and $R\bar{3}$ is often difficult [6–8].

0953-8984/90/367373 + 14 $03.50

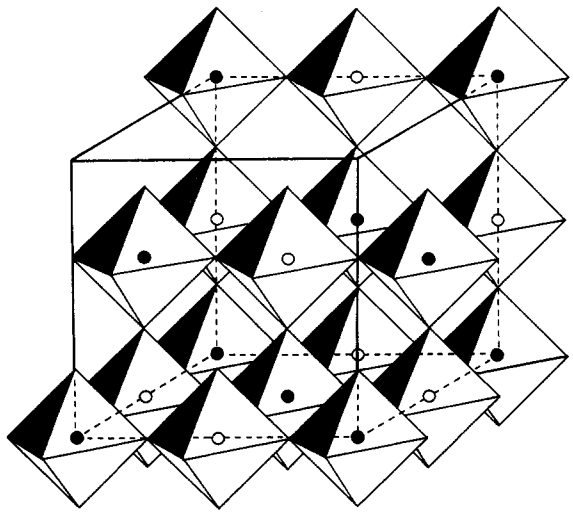

Figure 1. A schematic representation of the structure of $M^{II}M'^{IV}F_6$ mixed fluorides, showing the ordered three-dimensional arrangement of corner-sharing $M^{II}(M'^{IV})F_6$ octahedra: ● M^{II}, ○ M'^{IV}.

In spite of the numerous experimental studies devoted to these systems, a self-consistent description of the mechanism for the ferroelastic $Fm\bar{3}m \leftrightarrow R\bar{3}$ transition is not yet available, which is rather surprising with regard to the simple structural arrangement of these materials. In this context, we have undertaken a systematic study of two members of the $M^{II}M'^{IV}F_6$ series with NaCl packing, namely $CoZrF_6$ and $ZnZrF_6$ [9]. For $CoZrF_6$, the transition from $Fm\bar{3}m$ to $R\bar{3}$ has previously been observed at T_c = 273 K whereas for $ZnZrF_6$ the rhombohedral $R\bar{3}$ phase is stable at room temperature [2]. Our results are presented in a series of three papers, hereafter referred to as I to III; this paper (I) is devoted to a structural investigation, paper II to the dynamical approach of the phase transition by means of Raman and Brillouin scattering measurements, and finally a phenomenological description of the transition mechanism in the framework of Landau theory is presented in III.

In the present paper (I), we report the structural determination of $CoZrF_6$ through the ferroelastic phase transition, obtained by means of powder neutron diffraction profile refinements and of x-ray diffuse scattering experiments performed at room temperature. A preliminary study of $ZnZrF_6$ by means of powder x-ray diffraction is also presented. The neutron diffraction technique has been used for the structural determination because the position of fluorine atoms can be determined with a better accuracy owing to the high value of fluorine scattering factor.

2. Crystal chemistry

Powdered samples of $CoZrF_6$ ($ZnZrF_6$) have been synthesised by solid-state reaction at ~1020 K between stoichiometric amounts of CoF_2 (ZnF_2) and ZrF_4. The starting materials were obtained by fluorination under an HF gas flow at ~870 K of the corresponding dichloride $CoCl_2$ or $ZnCl_2$ and of ZrO_2 mixed with an excess of NH_4HF_2, respectively. The compounds were handled in an anhydrous controlled atmosphere, because of their very high hygroscopicity.

Single crystals of $CoZrF_6$ were obtained by the Bridgman technique after melting at ~1470 K. Red-purple coloured crystals consisting of platelets or parallelepipeds up to

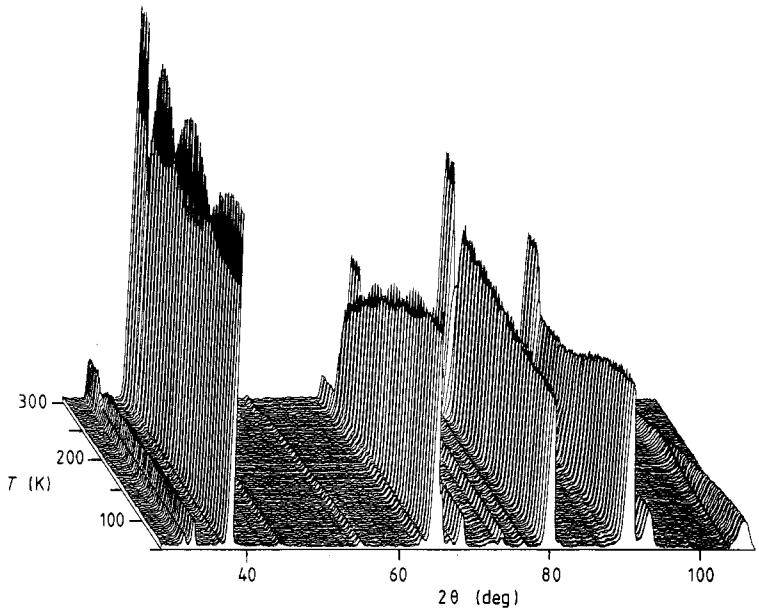

Figure 2. Temperature dependence of the $CoZrF_6$ powder neutron diffraction diagrams ($\lambda_0 = 2.522$ Å).

$5 \times 5 \times 5$ mm^3 in size exhibited natural faces perpendicular to the crystallographic cubic axes. Microcalorimetric and differential thermal analysis (DTA) measurements have confirmed the existence of a phase transition at $T_c = 272 \pm 1$ K (on heating); this transition is strongly of first-order and breaks the single-crystal samples.

No single crystal of $ZnZrF_6$ could be obtained at room temperature; as a matter of fact, the transition, which is also destructive for single-crystal samples, is detected by DTA at $T_c = 310 \pm 1$ K (on heating).

As a consequence, for both compounds, all experiments concerning the low-temperature rhombohedral phase were performed on powdered samples.

3. Experimental results

3.1. Neutron diffraction

Neutron diffraction measurements on powdered $CoZrF_6$ samples have been performed on the D1B two-axes powder diffractometer at the Institut Laüe–Langevin (ILL, Grenoble) [10] in a temperature range (50 to 300 K) including the domains of stability of the cubic and rhombohedral forms (figure 2). An angular range $28° \leqslant 2\theta \leqslant 108°$ has been chosen, with steps of 0.2°; an incident wavelength of 2.522 Å has been selected using a graphite (0 0 2) monochromator, which provides a high neutron flux of 6.5×10^6 n cm^{-2} s^{-1}. At low temperatures, 16 reflections have been observed, over the 19 expected ones in this range of 2θ; all of them can be indexed in the rhombohedral symmetry. For convenience, the primitive rhombohedral unit cell ($Z = 1$) will be

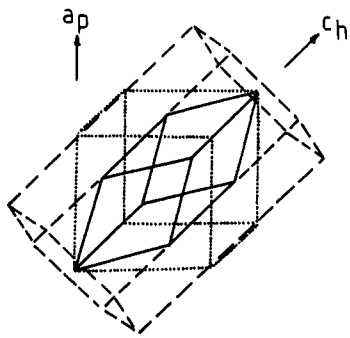

Figure 3. Relations between the cubic (dotted lines), rhombohedral (full lines) and hexagonal (broken lines) unit cells.

described in the hexagonal system, implying a multiplicity of 3 (figure 3). The relationships between rhombohedral and hexagonal cell parameters are the following:

$$\begin{aligned} a_h &= 2a_r \sin(\alpha_r/2) \\ c_h &= a_r[3(1 + 2\cos\alpha_r)]^{1/2} \end{aligned} \tag{1}$$

where a_h and c_h are the hexagonal lattice parameters and a_r and α_r the rhombohedral ones. On the other hand, the rhombohedral lattice can also be described with a pseudo-cubic unit cell implying a multiplicity of 4 (figure 3), whose parameters a_p and α_p are related to the previous ones by

$$\begin{aligned} a_p &= a_r(3 - 2\cos\alpha_r)^{1/2} \\ \cos\alpha_p &= (1 - 2\cos\alpha_r)/(2\cos\alpha_r - 3) = ((c_h/a_h)^2 - 6)/((c_h/a_h)^2 + 12). \end{aligned} \tag{2}$$

It should be noted that the symmetry is cubic when $c_h/a_h\sqrt{6} = 1$.

The structure determinations have been started with the data collected at 50 K, using the Young program [11] available at the ILL, which is based on the Rietveld method [12]. The observed and calculated neutron diffraction profiles at 50 K are compared in figure 4, and the corresponding structural data are summarised in table 1. It should be noted that the structure refinement has been performed by assuming isotropic thermal factors for the Co and Zr cations, owing to their centred position in the $Co(Zr)F_6$ octahedra and to the slight distortion found for these octahedra. Isotropic thermal factors have also been taken for the fluorine atoms, with regard to the limited number of Bragg peaks observed with this incident wavelength. Nevertheless, the assignment of the $R\bar{3}$ space group for $CoZrF_6$ at 50 K seems unambiguous with regard to the very low reliability factors R (table 1).

Structure determinations have been carried out for 75 different temperatures up to 300 K, using a cycling procedure of the Young program [11]. Refinements have been performed with constant isotropic thermal factors for all atoms, as determined at 50 K. Very low R factors are still obtained for all temperatures ($2 < R_{nucl} < 3$ and $3 < R_{prof} < 5$) (see table 1 for the definitions of R_{nucl} and R_{prof}), which confirms the existence of $R\bar{3}$ space group up to ~270 K. One can note also that the cell parameters and positional parameters of the fluorine atoms are in good agreement with those of the $FeZrF_6$ homologue, as determined previously by Mayer *et al* [13].

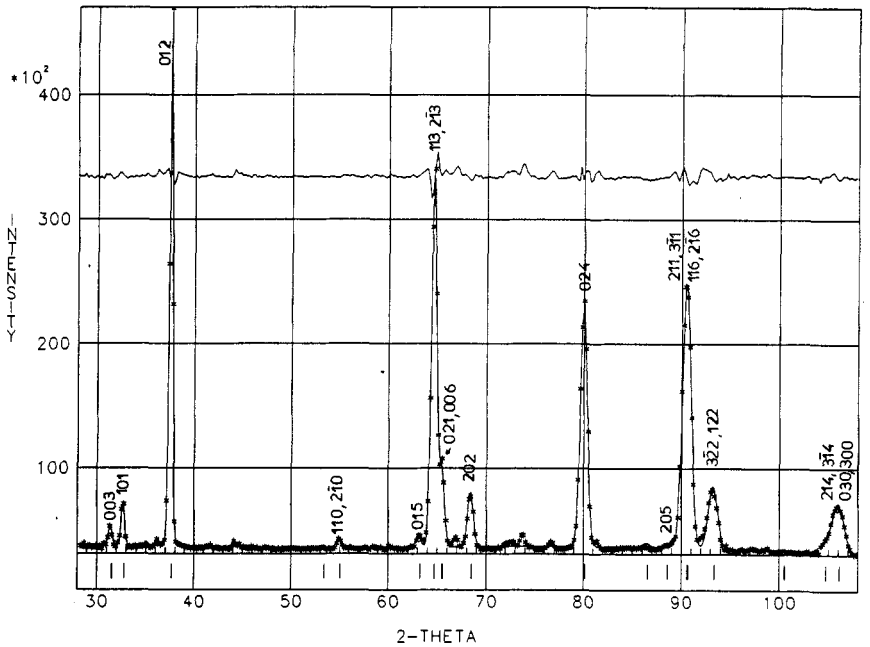

Figure 4. Observed (crosses) and calculated (full curve) powder neutron diffraction profiles of $CoZrF_6$ at 50 K. The upper curve shows the difference between observed and calculated profiles ($\lambda_0 = 2.522$ Å). The indexation of Bragg peaks refers to the hexagonal setting.

Table 1. Structural parameters of $CoZrF_6$ at 50 K in the $R\bar{3}$ space group with hexagonal description. The R factors are defined by

$$R_{nucl} = 100\,\Sigma|I(\text{obs}) - SI(\text{calc})|/\Sigma I(\text{obs})$$
$$R_{prof} = 100\,\Sigma|Y_i(\text{obs}) - SY_i(\text{calc})|/\Sigma Y_i(\text{obs})$$

where I(obs) and I(calc) are the observed and calculated integrated intensities of reflections, Y_i(obs) and Y_i(calc) are observed and calculated intensity data points and S is a scale factor. All thermal motions have been assumed to be isotropic; the B_{ii} are defined by $B_{ii} = 8\pi^2\langle u\rangle_{ii}^2$ and are given in Å^2. Standard deviations are given in parentheses.

a_h (Å)	c_h (Å)	V_{hex} (Å^3)	Co–F (Å)	Zr–F (Å)	α(Co–F–Zr) (deg)	$\tilde{\alpha}$(F–M–F) (deg)
5.466(1)	13.982(2)	362.0(3)	2.016(5)	2.007(5)	154(1)	89.4(5)

Atom		x/a	y/b	z/c	B
3 Co	(a)	0	0	0	0.10(5)
3 Zr	(b)	0	0	0.500	0.10(5)
18 F	(f)	0.084(1)	0.333(1)	0.084(1)	0.75(5)

$R_{nucl} = 2.44$ $R_{prof} = 3.20$

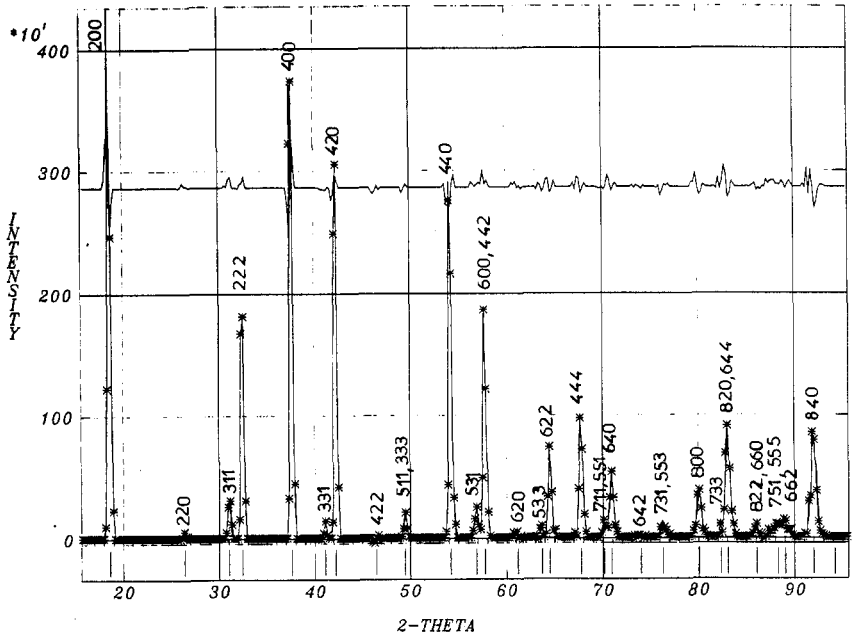

Figure 5. Observed (crosses) and calculated (full curves) powder neutron diffraction profiles of $CoZrF_6$ at 300 K. The upper curve shows the difference between observed and calculated profiles ($\lambda_0 = 1.285$ Å). The indexation of Bragg peaks refers to the cubic setting.

Another experiment has been carried out on powdered $CoZrF_6$ at 300 K in the cubic phase, with the D1B diffractometer equipped with a (3 1 1) germanium monochromator selecting thus an incident wavelength of 1.285 Å with a neutron flux of 0.4×10^6 n cm^{-2} s^{-1}. An angular range of $14° \leqslant 2\theta \leqslant 94°$ with steps of 0.2° has been chosen. In these conditions the 27 expected reflections consistent with a face-centred cubic structure have been collected (figure 5). The structure refinement has also been carried out with the Young program; the $Fm\bar{3}m$ space group with the fluorine atoms located in 24(e) Wickoff positions [14] leads to acceptable R factors (table 2). Anisotropic thermal factors have been taken into account for the fluorine atoms, whereas isotropic thermal factors have been assumed for the Co and Zr cations.

3.2. *X-ray diffraction*

Complementary results have been obtained with powdered samples of $ZnZrF_6$, using x-ray diffraction, in the temperature range 80–320 K, covering the stability domains of the cubic and rhombohedral phases. The experiments have been made with either a Secasi or a Philips counter diffractometer, using Cu K_α radiation and with scanning speeds of 0.1 and 0.5° min^{-1} (in θ), respectively. Silicon was used as an internal standard.

As previously mentioned, powdered $ZnZrF_6$ is very hygroscopic; in spite of the great caution taken in handling the samples, the data were often polluted by the presence of hydrolysis products formed during such time-consuming experiments. Thus, the structure determination could not be carried out in this case. Nevertheless, the diffraction patterns observed (figure 6) and the cell parameters calculated by mean-square refinement of Bragg peak positions showed a similar behaviour as for $CoZrF_6$ (table 3).

Table 2. Structural parameters of $CoZrF_6$ at 300 K, in the $Fm\bar{3}m$ space group. Co and Zr thermal motions have been assumed to be isotropic. The R factors are defined in table 1. Standard deviations are given in parentheses.

a_{cub} (Å)	V_{cub} (Å^3)	Co–F (Å)	Zr–F (Å)			
7.989(1)	510.0(2)	2.038(5)	1.971(5)			
Atom	x/a	y/b	z/c	$B_{11}(B)$	B_{22}	B_{33}
4 Co (a)	0	0	0	2.0(5)	—	—
4 Zr (b)	0.50	0.50	0.50	0.5(2)	—	—
24 F (e)	0.252(1)	0	0	1.1(3)	3.5(2)	3.5(2)

$R_{nucl} = 7.74$ $R_{prof} = 7.74$

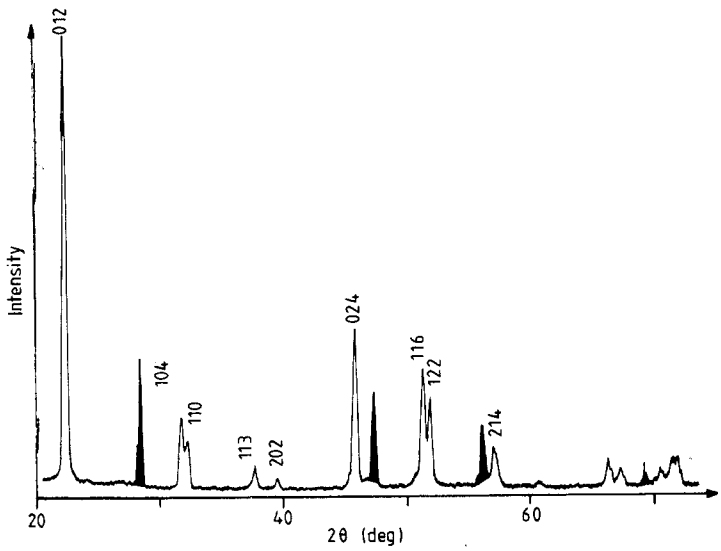

Figure 6. The $ZnZrF_6$ powder x-ray diffraction diagram at 300 K ($\lambda_0 = 1.5406$ Å). The shaded peaks correspond to silicon used for calibration. The indexation of Bragg peaks refers to the hexagonal setting.

Table 3. Lattice parameters of $ZnZrF_6$ in the cubic phase ($Fm\bar{3}m$) at 320 K and in the rhombohedral phase ($R\bar{3}$) at 300 K (hexagonal setting).

T (K)	Space group	a_{cub} (Å)	V_{cub} (Å^3)	
320	$Fm\bar{3}m$	7.988(2)	509.7(6)	
T (K)	Space group	a_h (Å)	c_h (Å)	V_{hex} (Å^3)
300	$R\bar{3}$	5.551(2)	13.936(8)	371.9(2)

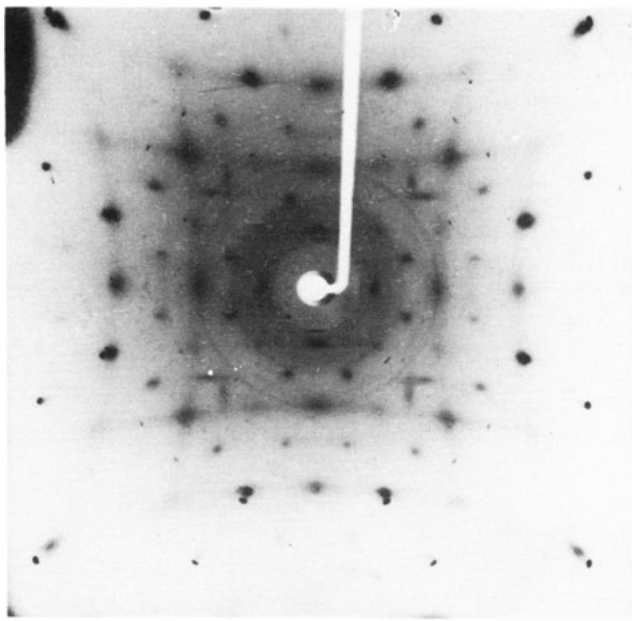

Figure 7. X-ray diffuse scattering patterns of $CoZrF_6$ single crystal at 300 K. The photograph corresponds to a fixed crystal with the incident x-ray beam parallel to the [001] direction. The [010] axis is vertical and the [100] one is horizontal.

3.3. X-ray diffuse scattering

X-ray diffuse scattering experiments have also been performed on $CoZrF_6$ single crystals at room temperature, i.e. in the cubic phase. The fixed crystal photographic technique has been used, with a precession camera operating with monochromatised Mo K_α radiation. Diffuse scattering patterns could be clearly observed after exposure times of about 4 to 6 days with an incident power of 1.5 kW on a platelet of about $0.2 \times 0.2 \times 0.05$ mm^3 size.

The diffuse scattering patterns (figure 7) consist of diffuse streaks parallel to the three cubic reciprocal directions and diffuse planes perpendicular to these directions. The diffuse streaks parallel to the ⟨001⟩ reciprocal row lines (direction of the incident x-ray beam) give rise to diffuse spots on the photographs, corresponding to their intersections with the Ewald sphere, and those parallel to ⟨100⟩ and ⟨010⟩ reciprocal row lines appear as small line segments where they intersect the Ewald sphere (figure 7). In addition, we notice the presence of [010] and [100] diffuse planes parallel to the x-ray beam direction (continuous lines corresponding to the intersection of these planes with the Ewald sphere). Because of cubic symmetry, one would also expect the presence of [001] diffuse planes, yielding concentric circles on the photographs; for experimental reasons due to the platelet shape of the crystal and because of the weak intensity of the diffuse planes, the expected [001] ones cannot be clearly observed.

These patterns closely resemble those reported several years ago by Denoyer *et al* in the cubic perovskites $NaNbO_3$ and $KMnF_3$ [15–17]. Indeed, $CoZrF_6$ exhibits the same three-dimensional arrangement of corner-sharing octahedra as in perovskites, excepted

for the ordering of Co and Zr atoms in these octahedra, responsible for the NaCl-type superstructure ($Fm\bar{3}m$ space group instead of $Pm\bar{3}m$ in the perovskite).

Thus, following the interpretation of Denoyer *et al*, which is based on a model calculation of the diffuse intensities [16, 17], we assign the diffuse streaks to structural disorder coming from rotations of the $Co(Zr)F_6$ octahedra around the main cubic axes, giving rise in real space to the existence of two-dimensional short-range correlations. In the perovskites, these distortions are related to zone-boundary rotatory modes, which create locally a unit-cell doubling, but in $CoZrF_6$ they represent zone-centre modes, because the cell doubling is already effective due to the ordering of Co and Zr cations, as previously mentioned.

As for the diffuse planes, such behaviour implies the existence of 'linear' disorder (one-dimensional short-range correlations in real space) assigned essentially by Denoyer *et al* [15–17] to displacements of the cations in octahedra (Co and Zr cations in our case).

4. Discussion

In figure 8 is given the temperature dependence of the lattice constants a_h and c_h (hexagonal description) of $CoZrF_6$ through the cubic-rhombohedral transition, together with the corresponding unit-cell volume. Abrupt changes can be seen for all data at T_c, confirming the first-order character of the transition. In the low-temperature phase, a_h slowly increases with increasing temperature, as expected for normal thermal expansion of the lattice; in contrast, c_h decreases simultaneously, which means that the spontaneous strain decreases when the transition temperature is approached from below.

From the temperature dependence of the structure of $CoZrF_6$, it is possible to describe the cubic–rhombohedral phase transition on quantitative grounds, through the thermal evolution of three parameters that fully characterise the extent of lattice distortion in the rhombohedral phase. These parameters are the following:

(i) The spontaneous strain e_s, defined as $\cos \alpha_p$, where α_p is the characteristic angle of the pseudo-cubic unit cell mentioned above (see relations (2) (figure 9(*a*)).

(ii) The rotation of the $Co(Zr)F_6$ octahedra around the threefold axis, which is characterised by a coordinate R related to the Co–F–Zr angle (α_R):

$$R \simeq \bar{d} \cos (\alpha'_R/2) \tag{3}$$

where $\bar{d}$ is the average Co(Zr)–F bond length, and α'_R is the projection of α_R on the (a_h, b_h) plane perpendicular to the threefold axis (figure 9(*b*)).

(iii) The internal deformation of the $Co(Zr)F_6$ octahedra, specified by a coordinate Q, which is related to the F–Co(Zr)–F angle α_Q (figure 9(*c*)).

The strain e_s is a macroscopic parameter determined directly from the positions of Bragg peaks; it is then directly related to the a_h and c_h lattice parameters (see relations (1) and (2)). This dimensionless parameter describes the rhombohedral distortion of the NaCl-type superstructure defined by the cationic arrangement, i.e. it is related to the cation-relative displacements within a single domain of the ferroelastic $R\bar{3}$ phase. R and Q are structural parameters determined from the positions of fluorine atoms in the unit cell. They represent the displacements of fluorine atoms with respect to their position in the cubic phase, which are induced by octahedra rotations around the threefold axis and by octahedra internal deformations, respectively. For the evaluation of these parameters, an average and constant Co(Zr)–F bond length $\bar{d} = 2.0$ Å has

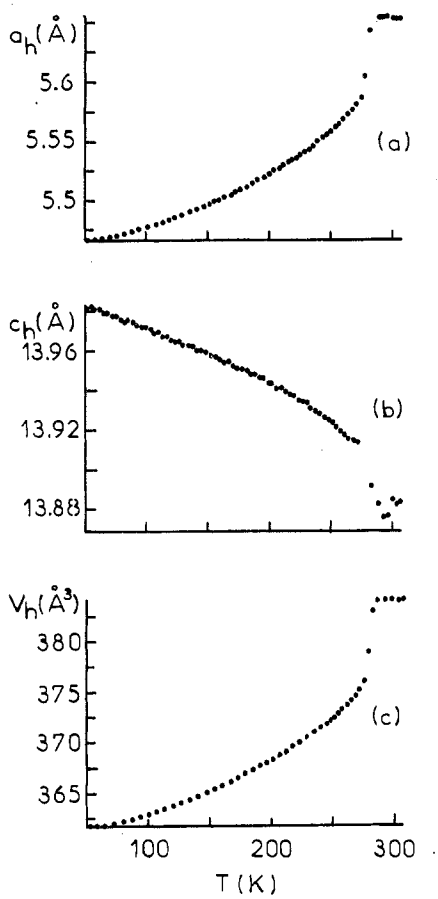

Figure 8. Temperature dependence of hexagonal unit-cell constants of $CoZrF_6$: a_h (*a*), c_h (*b*) and of the corresponding volume V_h (*c*). See text for the definition of a_h and c_h.

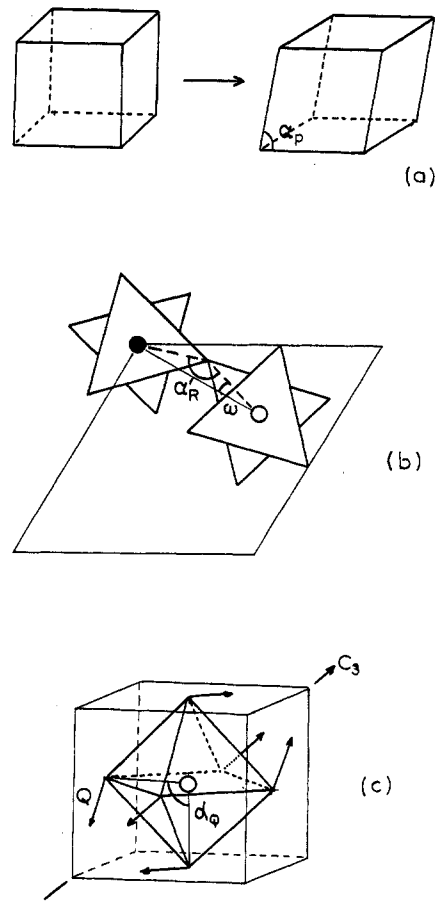

Figure 9. Schematic description of the spontaneous strain e_s (*a*), of the octahedra rotation R (*b*) and of the octahedra internal deformation Q (*c*).

been assumed (tables 1 and 2). As a matter of fact, the error introduced by such an approximation is negligible compared with the uncertainties on the corresponding measured angles (5% for α_R and 30% for α_Q).

Figure 10 shows the thermal evolution of e_s, R and Q. The best accuracy is obtained for e_s; one can note that the maximum value for R, measured at 50 K, corresponds to a rotation angle $\alpha_R \simeq 154°$, whereas Q values always remain very small (maximum deformation angle $\alpha_Q \simeq 89.4°$ at 50 K). All three parameters exhibit monotonic variations with temperature in the rhombohedral phase. Afterwards they abruptly vanish at the transition temperature to the cubic phase (first-order phase transition). So, they behave as order parameters for the phase transition and their behaviour will be analysed in more detail in the framework of Landau theory developed in paper III.

In order to test the mutual consistency of these data, we have considered the ideal case where the $Co(Zr)F_6$ octahedra are rigid bodies with perfect octahedral symmetry. In such a case, and considering again that the Co(Zr)–F bond lengths are quasi-identical

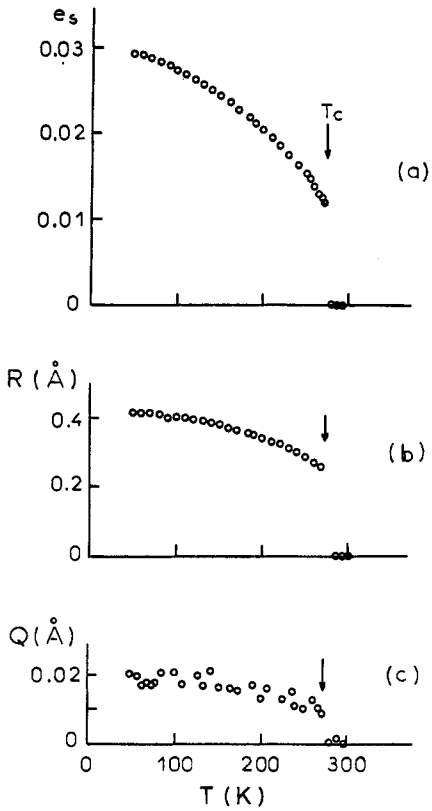

Figure 10. Evolution with temperature of the spontaneous strain e_s (*a*), of the octahedra rotation coordinate R (*b*) and of the octahedra internal deformation coordinate Q (*c*).

(tables 1 and 2), there exists a simple relation [18, 19] between the rotation angle of the octahedra $\omega = \pi/2 - \alpha'_R/2$ (figure 9(*b*)) and the lattice parameters (figure 8):

$$(c_h/a_h)^2 = 6/\cos^2\omega = 9/4\sin^2(\alpha_r/2) - 3. \tag{4}$$

Consequently, the rhombohedral angle α_r can be expressed as a function of the Co–F–Zr angle α_R [18, 19]:

$$\alpha_r = \cos^{-1}[(5 + \cos\alpha_R)/(6 - 2\cos\alpha_R)]. \tag{5}$$

Figure 11 shows the plot of the function (5) compared with the experimental points obtained with $CoZrF_6$ at different temperatures in the rhombohedral and cubic phases. In the rhombohedral phase, there are systematic and significant deviations of the data points with respect to (5), showing that the $Co(Zr)F_6$ octahedra are not perfect rigid bodies, so that the measured rotation angle ω is less than expected in the rigid case. Indeed, we have been able to measure such octahedra internal distortion (coordinate Q) whose temperature dependence (figure 10(*c*)) agrees qualitatively with that of the departure from perfect rigidity (figure 11). It should be noted however that in rhombohedral $CoZrF_6$, the departure from rigid behaviour always remains very small. Similar coupling between R and Q occurring in rhombohedral perovskites has already been discussed in some detail [20].

It is also worth noting that in the cubic phase the sum of theoretical ionic radii (8.13 Å) [21] is significantly higher than the observed lattice constant (7.99 Å). This

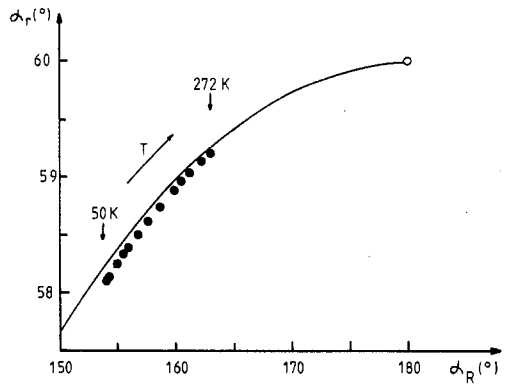

Figure 11. The α_r rhombohedral angle versus the α_R Co–F–Zr angle. Open and full circles correspond to the data points obtained in the cubic and rhombohedral phases, respectively; the full line is a plot of relation (5).

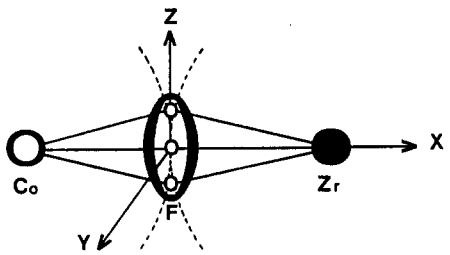

Figure 12. Schematic representation of the fluorine thermal ellipsoids in $CoZrF_6$ at 300 K, together with the split-atom model [13].

means that the instantaneous positions of fluorine atoms do not lie exactly on Co–Zr axes, as supported by the strong anisotropic thermal factors of these atoms (table 2). The fluorine thermal ellipsoids exhibit two equivalent long axes along the Y and Z directions, and a much shorter one along X, which corresponds to the Co–Zr bond direction. Such thermal ellipsoids can be interpreted in terms of a split-atom model [13], in which the fluorine atoms are statistically distributed between at least four equivalent positions, in order to generate an averaged position in 24(e) (figure 12). Such a model has also been proposed to take into account the entropy of transition in other $MM'F_6$ [8] and in perovskite-related fluorides [22]. As far as the $Co(Zr)F_6$ octahedra can be considered essentially as rigid bodies, the jump motions of fluorine atoms from one instantaneous position to another one would in fact be associated with reorientational motions of the octahedra around the cubic fourfold axes, from one tilted orientation to another one. This picture is in full agreement with the x-ray diffuse scattering patterns reported in section 3.3. Thus, according to this model, the cubic–rhombohedral transition exhibits some order–disorder character associated with $Co(Zr)F_6$ octahedra reorientations. Indeed, the rhombohedral phase may be seen as a frozen state of the disordered cubic phase, where the octahedra rotations around the three principal cubic directions freeze with equal amplitudes, thus preserving the threefold symmetry. However, an important displacive contribution in the transition mechanism is also clearly evidenced through the temperature evolution of the coordinate R (figure 10(b)).

Finally, it should be pointed out that the preliminary results obtained with $ZnZrF_6$, by means of x-ray diffraction, show that the thermal evolution of the spontaneous strain e_s in the rhombohedral phase determined from Bragg peak positions exhibit a similar behaviour as that reported in figure 10(a) for $CoZrF_6$ [9].

5. Conclusions

Neutron diffraction experiments performed on $CoZrF_6$ have shown that this compound undergoes at 272 K a first-order structural phase transition from a cubic high-temperature phase with $Fm\bar{3}m$ symmetry to a rhombohedral low-temperature modification with $R\bar{3}$ space group. From simple symmetry considerations, this transition is ferrodistortive (it occurs at the centre of the first Brillouin zone) and it is ferroelastic (it involves a change of the crystal system).

From the structural determination of $CoZrF_6$ at different temperatures through the phase transition, three order parameters that completely characterise the extent of lattice distortion in the rhombohedral phase have been measured, namely the spontaneous strain e_s, the coordinate of rotation of the $Co(Zr)F_6$ octahedra around the threefold axis, R, and the internal deformation coordinate of the octahedra, Q. The results show important thermal variations of e_s and R, but the Q coordinate always remains very small, showing that the $Co(Zr)F_6$ octahedra exhibit only small distortion from perfect octahedral symmetry. Thus, a displacive contribution in the transition mechanism due to octahedra rotations is clearly confirmed.

X-ray diffuse scattering experiments performed on $CoZrF_6$ are consistent with the existence of disorder in the cubic phase, due to reorientations of the $Co(Zr)F_6$ octahedra around the fourfold cubic axes; so, an order–disorder contribution may also be present in the transition mechanism.

Preliminary x-ray diffraction results show a similar behaviour for $ZnZrF_6$ homologue, as far as the spontaneous strain e_s is concerned.

Acknowledgments

The authors wish to thank Dr L Rabardel and J Villot (Laboratoire de Chimie du Solide du CNRS, University of Bordeaux I) for performing the calorimetric measurements. We are also indebted to Dr N B Chanh and Professor C Hauw (Laboratoire de Cristallographie et de Physique Cristalline, University of Bordeaux I) for their help during the x-ray diffraction and diffuse scattering experiments, and enlightening discussions.

References

[1] Babel D 1967 *Struct. Bonding* **3** 5
[2] Babel D and Tressaud A 1985 *Inorganic Solid Fluorides* ed P Hagenmuller (New York: Academic) p 97
[3] Teufer G 1956 *Acta Crystallogr.* **9** 539
[4] Burns J H 1962 *Acta Crystallogr.* **15** 1098
[5] Reinen D and Steffens F 1978 *Z. Anorg. Allg. Chem.* **441** 63
[6] De Beer W H J, Heyns A M, Richter P W and Clark J B 1980 *J. Solid State Chem.* **33** 283
[7] De V Steyn M M, Heyns A M and English R B 1984 *J. Cryst. Spectr. Res.* **14** 505
[8] Heyns A M and Pistorius C W F T 1974 *Spectrochim. Acta* A **30** 99; 1975 *Spectrochim. Acta* **31** 1293; 1976 *Spectrochim. Acta* A **32** 535
[9] Rodriguez V 1989 *Thesis* University of Bordeaux I
[10] Blank H and Maier B (ed) 1988 *Guide to Neutron Research Facilities at the ILL* (Institut Laüe Langevin) p 14
[11] Wiles D B and Young R A 1982 *J. Appl. Crystallogr.* **15** 430
[12] Hewat A W 1973 *Harwell Report* AERE-R 7350
[13] Mayer H W, Reinen D and Heger G 1983 *J. Solid State Chem.* **59** 213

[14] Hahn T (ed) 1983 *International Tables for Crystallography* (Dordrecht: Reidel) p 678
[15] Denoyer F, Comes R and Lambert M 1971 *Acta Crystallogr.* A **27** 414
[16] Denoyer F, Comes R, Lambert M and Guinier A 1974 *Acta Crystallogr.* A **30** 423
[17] Denoyer F 1977 *Thesis* University of Paris-Sud (Orsay)
[18] Moreau J M, Michel C, Gerson R and James W J 1970 *Acta Crystallogr.* B **26** 1425
[19] Michel C, Moreau J M and James W J 1971 *Acta Crystallogr.* B **27** 501
[20] Megaw H D and Darlington C N W 1975 *Acta Crystallogr.* A **31** 151
[21] Shannon R D 1976 *Acta Crystallogr.* A **32** 751
[22] Moriya K, Matsuo T, Suga H and Seki S 1977 *Bull. Chem. Soc. Japan* **50** 1920; 1979 *Bull. Chem. Soc. Japan* **52** 3152